

The Optics of Shadow Bands

Branko Sretenović

Independent researcher, Serbia
e-mail: [Mathallica] mathallica3@outlook.com

Preprint version 2
© 2026 Branko Sretenović

July 3, 2026

Abstract

Shadow bands are transient, rippling patterns of light and dark that may appear in moments before and after totality in a solar eclipse. Despite centuries of reports, their physical origin has remained unresolved. This preprint develops a geometric-optical solution in which the Sun's extended structure produces a celestial analogue of Young's double-slit experiment, generating an interference-like intensity pattern on the ground, modulated by Earth-atmosphere effects. The analysis combines solar limb geometry, atmospheric propagation effects, and a wave-based formulation that yields quantitative predictions for fringe width and spacing. The resulting model accounts for the principal observational features of shadow bands and clarifies why the phenomenon is both elusive and highly sensitive to viewing conditions. A more detailed and pedagogical exposition of this framework appears in the author's book *The Optics of Shadow Bands* (2025).

KEYWORDS: shadow bands, solar eclipse, double-slit interference, fringe formation, wave propagation, solar limb darkening, geometric optical model

Introduction

Shadow bands are transient, centimeter-scale fluctuations of light and dark that appear on the ground in the moments before and after totality during a solar eclipse. Although reported for more than two centuries, their physical origin remains unresolved. Observations show variability in visibility, spacing, motion, and contrast, and existing explanations account for only subsets of these features. No quantitative, predictive framework has been established.

Previous attempts, including atmospheric-turbulence models such as Codona's, reproduce certain qualitative aspects but do not yield quantitative predictions for fringe spacing or directional motion, nor do they identify the underlying physical cause in the solar-atmospheric system. These limitations motivate the geometric-optical model based on solar-limb geometry and wave-based propagation developed in the sections that follow.

Similar banded patterns have occasionally been reported during other obscuration events, such as sunrise and sunset, suggesting a broader underlying mechanism.

1 Methods

The aim of this work is to identify the physical mechanism responsible for shadow bands and to derive approximate predictions for their observable width, spacing, and motion. The analysis

is theoretical and draws on established solar-limb geometry, optical principles, and documented observational constraints.

Atmospheric variability and solar-atmospheric irregularities can influence the appearance of shadow bands, introducing uncertainties that are not modeled in detail here. The focus is instead on the underlying geometric-optical mechanism that governs the formation and evolution of the bands under clear terrestrial conditions.

To establish that the physical analogue of shadow bands is the system of bright-dark fringes produced in a double-slit experiment, we treat the two bright solar shafts present at the verge of totality as the effective pair of coherent sources. Although the modern double-slit experiment is typically performed with a laser illuminating two slits in a darkened laboratory, such controlled conditions are not essential for the underlying physics. Young’s original demonstration—achieved with nothing more than a pane of glass and a thin card—already shows that a two-slit configuration can arise from simple, naturally occurring geometries.

For a double-slit interference pattern to form, several physical conditions must be met. The light must possess sufficient coherence to maintain a stable phase relationship across the two paths. Monochromatic, or at least quasi-monochromatic, illumination is strongly preferred, as a narrow spectral bandwidth preserves the phase stability required for high-contrast fringes. The apertures must be narrow, well-defined, and separated by a distance that allows their diffraction patterns to overlap on the observation plane. The screen must lie far enough from the slits for the diffracted waves to spread and interfere, and the environment must be sufficiently stable and darkened to preserve fringe contrast. Under these preconditions—even with minimal equipment, as in Young’s demonstration—the characteristic bright-dark fringe system emerges with clarity.

Beyond establishing the analogy between shadow bands and double-slit fringes, the model must also satisfy additional observational constraints, including the temporal evolution, directional motion, altitude dependence, and sensitivity to surface texture reported in eclipse observations. These constraints guide the geometric-optical formulation developed in the sections that follow.

2 Observational Constraints

Shadow bands do not always appear during a total solar eclipse. When they do, they emerge at specific time intervals—typically just before totality (C2, *second contact*)—before vanishing during totality. They reappear after totality (C3, *third contact*) and disappear again after another interval. Observations suggest varying time intervals. However, they always disappear during totality.

In some cases, shadow bands disappear, and in other cases, they reappear. Sometimes they appear as faint parallel alternating light and dark bands, and other times as curved, snake-like patterns. Recorded widths range from approximately 2.5 cm (1 in) to at least 46 cm (18 in), while their observed speed varies widely, from approximately 10 cm/s (4 in/s) to 180 cm/s (70 in/s). Their direction appears tangential to the Moon’s shadow. Observers have noted occasional variations in contrast.

To add more enigma, these features fluctuate as the Moon gradually obscures the Sun. Shadow bands tend to become more visible as the Sun’s crescent diminishes.

To ensure an exact and reliable understanding of shadow bands and their effect, the text will incorporate quotations and rephrased findings from authors whose research is widely recognized in the field. Additional references to reputable scientific papers will support and enrich the analysis with valuable insights.

Hence, these statements will be treated as trustworthy shadow bands observation facts. The observed facts are categorized according to the distinct properties of shadow bands and will later be compared with the corollaries derived from the proposed explanation, to validate its predictions.

2.1 Width and Spacing

Codona conducted an outstanding exploration of shadow bands and developed Scintillation theory, which offers a scientific explanation for their occurrence. In his *Sky and Telescope*, article *The Enigma of Shadow Bands* Codona (1991) presented a plot with time on the x -axis, and shadow band spacing on y -axis, illustrating how the spacing of shadow bands changes as totality approaches [5]. From the plot, we can infer that three minutes before totality, the shadow band spacing typically ranges from a few to about 10 centimeters. The range gradually shrinks and by one minute before totality the spacing ranges from approximately two to a few centimeters. In the final 20 seconds, the spacing increases more, with the pattern becoming intricate and richly detailed. On the verge of totality, the range of spacing shrinks to its minimum, but the spacing somewhat increases and is generally a few centimeters. Shadow bands become more distinctly visible. Nevertheless, the spacing may extend to half a meter, to meter, or even longer.

In the article *Visual, Photographic and Photoelectric Detection of Shadow Bands at the March 7, 1970, Solar Eclipse*, published in the international journal *Nature* in 1971, a team from the Department of Physics at Ball State University, Indiana, measured several characteristics of shadow bands, focusing on their orientation, width, spacing, and speed [13]. Teams of observers at evenly distributed locations around the Moon's shadow on Earth known as the *umbra*, collected information visually, photographically, and photoelectrically. The width and spacing of shadow bands varied widely. Reported spacing intervals ranged from 3 to 8 centimeters and from 15 to 20 centimeters while the individual band widths were typically just a few centimeters. Both width and spacing were observed to change over time.

2.2 Direction

Feldman (1938a), in his article *Shadow Bands – Part I* from *Popular Astronomy*, analyzed a substantial number of shadow band observations, focusing specifically on their direction [6, ADS link]. Here is the quote of a sentence from his conclusion.

A candid world must therefore accept my statement that the shadow bands are in every case where carefully observed, parallel to the nearest edge of the shadow and consequently a portion of a complete ring of bands.

In the article *Visual, Photographic and Photoelectric Detection of Shadow Bands at the March 7, 1970, Solar Eclipse* teams of observers at evenly distributed locations around umbra collected data about orientation of shadow bands. In summary, along the umbra central path of the eclipse (*totality path*), the shadow bands aligned tangentially with the eclipse shadow both before and after totality. However, at locations slightly off the centerline of totality path—yet still within the totality path—the bands were only approximately tangential, and in one instance, they exhibited significant rotation during the one-minute period of shadow band activity before totality.

Shadow bands may change direction and that was stated in a passage from the book *The Total Solar Eclipse, 1905* by British Astronomical Association published in 1906 [3].

Three minutes before totality they were going in a direction 22° west of south. A minute later they had swung round and were only 17° west of south. This rotatory movement has been noticed before, but it was fully verified on this occasion.

2.3 Related Phenomena

Stephen James O’Meara (2009) in his article *Secret Sky - Searching for Shadow Bands* from *Astronomy* describes his experience with shadow bands occurring when the Sun was not eclipsed by the Moon [21, Astronomy link]. He recognized shadow bands occurring when the Sun was partially eclipsed by a roof while he read his book. Shadow bands rippled diagonally over pages. In the other situation 15 minutes before sunrise, while he was in a jet at high altitude, he saw shadow bands on the jet’s wing.

In this instance of non-eclipse shadow bands, they appeared soon after sunrise and immediately before sunset. The quote is taken from the article *Observations of “Shadow Bands” without an Eclipse*, published in *Monthly Weather Review 1906* by Henry (1906) [12].

Heretofore this interesting and mysterious phenomenon has been observed only during the occurrence of solar eclipses, but by a very simple method M. Rozet has been able to make daily observations of the bands at sunrise and sunset. The light of the sun at the time of its appearance and disappearance behind somewhat lofty mountains on the horizon is received on a white screen, arranged in the observer’s room, and bands are produced apparently identical in character with those observed during an eclipse.

Shadow bands have been artificially generated, observed, and photographed by stars other than the Sun. These bands appear to share the same underlying cause as shadow bands seen during a total solar eclipse. Here are a few outlines from the Gaviola (1948) article *On Shadow Bands at Total Eclipses of the Sun* in *Popular Astronomy* [10, ADS link].

Shadow bands whose characteristics resemble the ones described are familiar to observing astronomers: they are seen when a bright star is in the field and eyepiece is removed, replacing it with the naked eye. Although easy to see, they are difficult to photograph.

[...]

Picture 1 was taken with light of β Centauri using the 12 cm focus camera and an exposure time of 1/10 second. Two shadow band system can be seen, having both the same wavelength, $L = 7$ cm, but different orientations: $S22^\circ W$ and $S65^\circ W$.

2.4 Occurrence

Observations typically document the time intervals during which shadow bands appear before totality and fade after it. These periods range from several seconds to a few minutes.

Feldman (1938a) in the article *Shadow Bands – Part I* wrote a paragraph where he stated that the shadow bands were clearly detected at the height of 3.8 kilometers during an eclipse. The shadow band width at the altitude was shorter than on the ground. He commented that the shadow bands were nearly tangential to the umbra.

The hearty cooperation of the Spanish government resulted in observations being secured from certain military balloons at Burgos, Spain, from which “white screens hang horizontally”... “In one of the balloons the bands were more clearly seen at the height of 3800 meters than on the ground, and were much finer (0.6 to 0.8 cm) and nearer together (1.2 to 1.6 cm), and had a velocity of 1.5 meters per second.” (On the ground the widths reported varied from 1 to 10 cm, and distance apart from 3 to 25 cm.) The direction reports came from eight different points, through Spain and Majorca, to Tripoli, and Rotch wrote: “The observations at different places indicate that the bands lay nearly tangent to an ellipse having for its longest diameter the width of the shadow, and representing all points where totality occurred at the same instant.”

A research team from the Department of Physics and Astronomy and the School of Engineering at the University of Pittsburgh, in collaboration with the Allegheny Observatory, investigated the possible atmospheric origin of shadow bands during August 21, 2017, total solar eclipse. Their findings were presented in a preprint titled *Observation of Eclipse Shadow Bands Using High Altitude Balloon and Ground-Based Photodiode Arrays* in 2020 [17]. The team deployed photodiode arrays both on the ground and aboard high-altitude balloons reaching approximately 25 km. Shadow bands were detected in both environments, with continuous and approximately the same fluctuations observed at high altitude and at ground level, suggesting that the phenomenon cannot originate solely within the Earth’s lower atmosphere.

Very few photographs of shadow bands have been found that haven’t been visually enhanced—typically by increasing contrast. Although shadow bands have been captured on video numerous times, they remain notoriously difficult to photograph. Even when successfully recorded, their features can be elusive and hard to interpret, often leading to confusion. Observers at the same location and moment have sometimes disagreed about what they witnessed.

That said, there are many unaltered shadow band videos available online. Their motion, once in play, eventually makes them discernible.

2.5 Shadow Band Theories

Let us now consider the most widely accepted explanation of shadow bands to date: the Scintillation theory. This hypothesis was proposed by Codona (1986), in a peer-reviewed article titled *The Scintillation Theory of Eclipse Shadow Bands*, published in *Astronomy and Astrophysics* [4].

Codona’s theory suggests that minute atmospheric irregularities cause light from the solar crescent to undergo scintillation, producing interference-like patterns of alternating light and dark bands on the ground just before and after totality. While the theory remains prominent, it is not without its critics. There are at least two reasons for maintaining healthy skepticism, and they are outlined below.

1. **Concentric Ring Formation.** Empirical studies from independent researchers suggest that shadow bands may form complete rings—some reportedly concentric around the umbra. However, it is unlikely that atmospheric disturbances consistently result in such organized motion. While air cooling may influence wind direction toward or away from the umbra’s center, its effect near the edges is likely minimal.
2. **High-Altitude Observations.** Codona’s theory attributes shadow band formation to atmospheric turbulence at altitudes below two kilometers. However, empirical evidence has challenged this assumption. Two independent studies—referenced earlier—have recorded shadow bands at significantly higher elevations: one at 3.8 km, and another at approximately 25 km. These findings suggest that the phenomenon may not originate solely within the lower atmosphere.

3 Model

The cause of shadow bands comprises the Sun’s layers, the Earth’s atmosphere, features of the umbra, and the properties of light.

The Sun and its atmosphere consist of several layers. For our investigation, we do not need to examine the layers within the Sun—only the one at its surface, that is the *Photosphere*.

The Sun’s limb refers to the outer edge of the Sun’s disk as observed from Earth. As one observes the Sun gradually approaching the limb, it appears darker.

The Sun's atmosphere consists of four layers: the *Temperature Minimum Region*, *Chromosphere*, *Transition Region*, and *Corona*. The Temperature Minimum Region is the Sun's lowest atmospheric layer, while the Corona is the uppermost.

The Temperature Minimum Region is often considered an integral part of the Chromosphere. However, it is sometimes regarded as a boundary between the Photosphere and Chromosphere.

This boundary plays an important role in the study of shadow bands. Hence, in this book the Temperature Minimum Region will specifically refer to a boundary—a distinct entity separate from the Chromosphere.

Although the Sun appears uniform to an observer on Earth, its layers are highly dynamic and emit varied illumination. Below is a brief overview of how bright each layer is in the Sun's surface and atmosphere:

1. **Photosphere.** By far the brightest layer.
 - **Sun limb.** The Sun disk appears darker at the limb due to observational perspective, yet it remains significantly brighter than any atmospheric layer.
2. **Temperature Minimum Region (Dark Band).** Darker than its surroundings.
3. **Chromosphere.** Initially bright, then gradually darkens.
4. **Transition Region.** The darkest of all layers in visible light.
5. **Corona.** Begins bright but quickly dims.

From here, we infer the presence of three brighter regions: the Sun disk, Chromosphere ring, and Corona ring. Since both the Chromosphere and Corona begin with bright regions when moving outward from the Sun's center, we will refer to these zones as the Chromosphere base and Corona base.

There is no proportionality of the Sun layers' widths in the illustration below (FIGURE 1); it represents their relative positions and shape only.

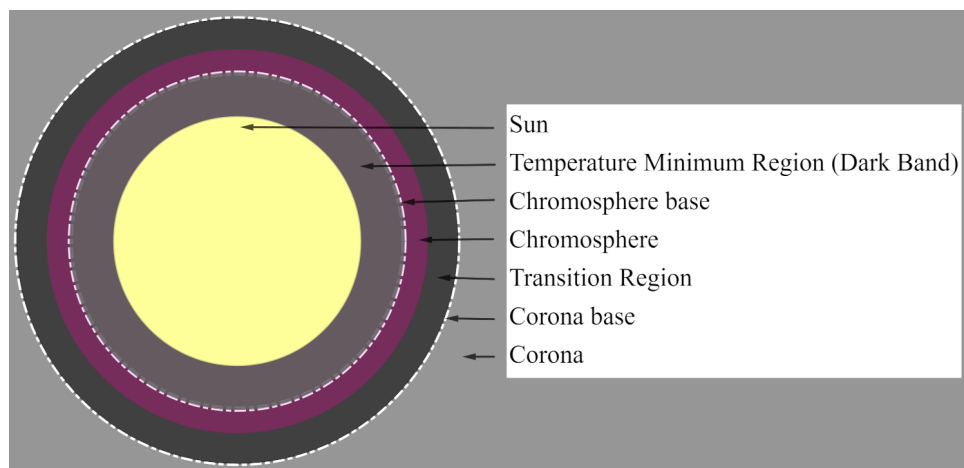


Figure 1: Bright Regions with High Contrast in Sun Layers

Bright strata with high contrast of the Sun and its atmosphere are:

- The Sun

- The Chromosphere base
- The Corona base

Compared to the Sun's surface, the Sun's atmosphere has lower intensity and is much less broadband. Each atmospheric layer contributes more specific and darker wavelengths having emphasized discrete spectrum.

3.1 Solar Atmosphere Layer Spectrum

The Photosphere, the Sun's outermost visible layer, is the primary source of outward-radiating photons. Its light is broadband, encompassing a full range of visible wavelengths. Due to its intense brightness and spectral richness, the Photosphere appears visually uniform, effectively concealing the solar atmosphere from direct observation. However, during an eclipse, when the Photosphere is obscured by the Moon, previously hidden layers—such as the Chromosphere and Corona—briefly emerge into view.

The central region of the Sun's disk appears brighter than its outer edge, a phenomenon known as *limb darkening*. This gradual dimming toward the limb arises from optical and geometric effects.

This effect of *optical depth* is fundamental to how different regions of the Sun manifest during an eclipse, contributing to the layered contrast that defines the solar edge.

Limb darkening is not unique to the Sun; many stars exhibit similar effects. As with our Sun, the intensity of emitted light typically decreases from the stellar center toward the limb due to optical depth and temperature gradients in the outer layers. Simultaneously, the spectral characteristics of stellar atmosphere become more pronounced at the limb of many stars, as they do at the Sun's limb.

Limb darkening is a precondition for the formation of shadow bands.

When observed through optical instruments, the Temperature Minimum Region is often referred to as the *Dark Band*. Since this study centers on optical phenomena, the term Dark Band will be used frequently throughout the book.

The Dark Band appears darker than the underlying solar surface—but more importantly, it is dimmer than the Chromosphere above. However, the Dark Band should not be perceived as truly dark, but rather as less bright compared to its surroundings.

As will be shown, the Dark Band plays a critical role in producing shadow bands.

The Chromosphere is an extremely dynamic and inhomogeneous layer of the Sun, and it remains only partially understood. It appears progressively darker as it is observed farther from the Sun's center.

Limb darkening enhances the visibility of the Chromosphere near the solar limb, where its spectral lines become more pronounced. However, these lines are not emphasized as strongly as those of the Corona, which lies above the Chromosphere and therefore closer to Earth's direct line of sight.

The Chromosphere plays a crucial role in generating shadow bands.

The Transition Region primarily emits ultraviolet light, which lies beyond human visual perception. As such, it appears dark within the visible spectrum—indeed, it is the dimmest layer among all solar strata at visible wavelengths.

The Transition Region—plays a subtle yet significant role in the appearance of shadow bands, but it will not be discussed in this document.

The Corona gets quickly darker as we look at it farther from the Sun center.

The Corona lines are emphasized in the Sun limb due to limb darkening. Its lines are more pronounced than the Chromosphere lines because the Corona is the topmost layer and therefore closer to the Earth.

The Chromosphere base and Corona base are tight to the Photosphere. When the Moon partially covers the Photosphere, it also partially covers the Chromosphere base and Corona base. Consequently, the brightest parts of the Sun surface and atmosphere during an eclipse arise from these three bases. We'll refer to them as three slivers:

- Sun sliver
- Chromosphere sliver
- Corona sliver

The Corona sliver is the least bright and we'll not analyze its contribution to the shadow bands formation.

3.2 Solar Atmosphere Layer Width

The extensions of the Sun's atmospheric layers will be presented as perceived from Earth's perspective, referring to them as widths.

Due to solar dynamics, dimensions such as layers' widths cannot always be determined with precision—sometimes carrying uncertainties of several hundred kilometers.

Accordingly, the mathematical derivations in this study will often rely on ranges and approximations, reflecting the variable nature of the parameters involved.

While the Photosphere's internal width is not central to this investigation, its visible disk—the apparent surface—defines the Sun's overall size.

We denote the radius of the Sun as

R - Sun radius

$$\begin{aligned} R &= 7 \times 10^5 \text{ km} \\ &= 7 \cdot 10^2 \cdot (10^3 \text{ km}) \\ &= 700 \text{ Mm} \end{aligned}$$

The limb zone is not strictly defined, but it is usually taken as outermost couple percents of Sun's radius.

The Temperature Minimum Region exhibits significant variability, even across relatively short solar segments. This layer, shaped by the Sun's dynamic behavior, can extend over bright mottles within the Chromosphere—or in some areas between the Sun and Chromosphere, may not manifest at all.

The Dark Band may extend up to 1 000 km above the solar surface, or contract to just a few hundred kilometers—if it forms at all.

For our analysis, we adopt an average thickness of 500 km, equivalent to 0.5 Mm.

Estimating the Chromosphere's width is inherently complex due to its dynamic and highly variable nature. Recall that In this preprint, we distinguish the Chromosphere from the Temperature Minimum Region.

The Chromosphere's brightness increases rapidly from the Dark Band (Temperature Minimum Region). It forms the brightest chromospheric features that we'll refer to as the *Chromosphere base*.

This stratum typically does not exceed 2 000 km (2 Mm) in altitude. For the purposes of this study, we adopt a vertical distance between the Temperature Minimum Region and the Chromosphere base of 400 km (0.4 Mm).

We estimate the full distance from the Chromosphere base to the solar surface by appending the average thickness of the Dark Band (0.5 Mm).

δ_3 - distance from Chromosphere base to Sun surface

$$\begin{aligned}\delta_3 &= 0.5 \text{ Mm} + 0.4 \text{ Mm} \\ &= 0.9 \text{ Mm}\end{aligned}$$

From the Chromosphere base forward, the brightness drops faster at first but then decreases slowly toward the Transition Region.

The maximum thickness of the Chromosphere is estimated not to exceed 2 500 km, though in some regions it may be several times thinner.

The Transition Region, which bridges the Chromosphere and the Corona, is exceptionally dynamic and structurally unstable.

Its thickness varies greatly across the solar disk and within active regions, often measuring only a few hundred kilometers.

The base of the Corona typically begins at an altitude of approximately 2 500 km above the Sun's surface (Photosphere), though local variations may shift this by several hundred kilometers.

The brightness of the Corona diminishes rapidly outward from its base, often following an approximate inverse-square law—where intensity decreases with the square of the radial distance from the Sun's center. As a result, the brighter portion of the Corona—referred to as the *Corona base*—is relatively narrow.

To estimate the distance from the Corona base to the Chromosphere base, we combine known layer altitudes:

d_1 - distance from Corona base to Chromosphere base

$$\begin{aligned}d_1 &= 2\,500 \text{ km} - \delta_3 \\ &= 2.5 \text{ Mm} - 0.9 \text{ Mm} \\ &= 1.6 \text{ Mm}\end{aligned}$$

FIGURE 2 denotes the Sun and its atmosphere strata with the high contrast along with the mutual distances. Notice that the Chromosphere base and Corona base are represented with a dashed line designating their dark gaps. The picture is descriptive, not drawn to scale.

s - circle representing Sun surface

s_2 - circle representing Chromosphere base

s_3 - circle representing Corona base

The distance from the Corona base to the Sun surface is

$$\begin{aligned}d_1 + \delta_3 &= 0.9 \text{ Mm} + 1.6 \text{ Mm} \\ &= 2.5 \text{ Mm}\end{aligned}$$

This distance is considerably smaller than the Sun's diameter that is

$$\begin{aligned}2R &= 2 \cdot 700 \text{ Mm} \\ &= 1\,400 \text{ Mm}\end{aligned}$$

We could say that the Corona and Chromosphere bases are tied to the Sun surface.

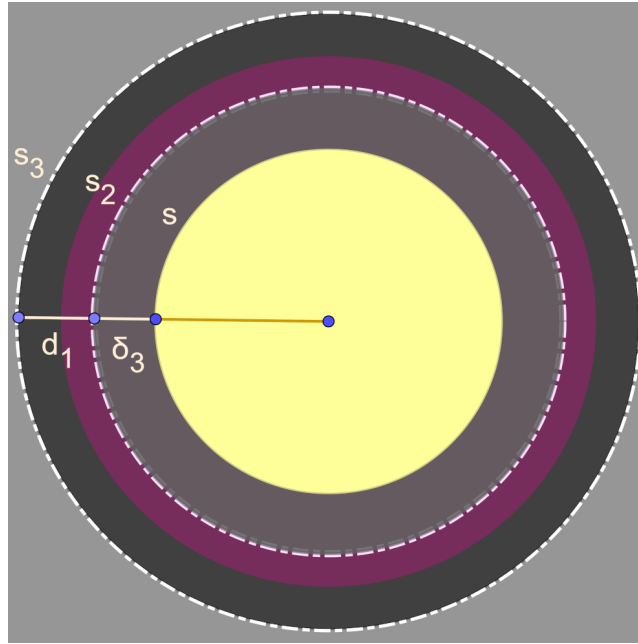


Figure 2: Bright Areas of Sun Surface and Atmosphere with Distance Labels

3.3 Geometric Model

Centuries of shadow band observations have revealed that optimal viewing conditions demand a flat, bright, and non-reflective surface with minimal light dispersion and moderate absorption. Typical examples include white sheets, projection screens, sidewalks, and similar materials.

We refer to any such suitable surface as the *shadow band observation surface*, or briefly, the *observation surface*.

For maximum visibility, the observation surface should be positioned perpendicularly to incoming sunlight rays, allowing the alternating light and dark patterns to form with greatest clarity.

As a solar eclipse progresses and the Sun is reduced to a thin sliver—only a fraction of an arcminute wide—ambient darkness deepens. Yet even then, the Sun remains Earth’s dominant light source.

The Moon’s shadow cast upon Earth’s surface the umbra. Its intense darkness reveals an elliptical form, shaped by celestial geometry.

As the Moon moves, its umbra travels along the path of totality—the shadow’s trajectory across Earth’s surface.

The umbra’s behavior also depends strongly on the angle of incoming sunlight at the observation surface, meaning both the shape and dynamics of the totality path can vary considerably.

The umbra’s diameter typically ranges from 100 km (60 mi) to 1 000 km (600 mi), with a common value of approximately 150 km (95 mi).

Near the equator, the lunar umbra travels across Earth at roughly 1 800 km/h (1 100 mi/h), while near the poles, speeds may reach up to 8 000 km/h (5 000 mi/h). A typical average is around 3 000 km/h (1 900 mi/h), though this can vary by a factor of two or more depending on location and geometry.

Light from various solar layers extends outward and grazes the umbra’s edge, forming the *penumbra*—a transitional zone where sunlight only partially reaches the surface, and brightness fades gradually.

For analytical clarity, we model the umbra as an ellipse, while acknowledging that subtle adjustments may be needed to account for real-world deviations and temporal changes driven by shifting orbital mechanics.

To illustrate how solar layer illumination affects the observation surface, FIGURES 3, 4 establish key spatial relationships.

u - ellipse representing umbra

The umbra center lies along the line connecting the centers of the Sun and Moon.

C - Sun center

M - Moon center

Point C is also center of the Chromosphere base and Corona base.

We can interpret the umbra's center as the projection of the Sun's and Moon's centers.

$C' = M'$ - projections of the Sun's and Moon's centers onto the umbra center

The *centerline* of the umbra is the midline running through its core during an eclipse.

From our chosen perspective given in FIGURE 4, the umbra moves horizontally, traveling from left to right. The movement direction is represented by a vector originating from the umbra's center. Therefore, the vector replaces the centerline, visually indicating the umbra's trajectory.

The center point of the observation surface is located near the umbra.

O - observation surface center point

From the observation surface's perspective, it perceives the Sun's and Moon's centers, along with their disks like in FIGURE 3.

s - disk representing Sun

m - disk representing Moon

Due to limb darkening, the brightest arc of the Sun sliver is the arc bordering the Moon's disk, referred to as the *Sun sliver base* or briefly *Sun base*. This arc is the brightest arc during an eclipse, influencing optical effects near totality.

Hence, the Sun sliver brightest point is on the Sun sliver base. Due to limb darkening, it is the closest point to the Sun center.

S_1 - brightest point of Sun base

A, B - intersections of Sun and Moon disks

$\widehat{AS_1B}$ - arc of Sun sliver base (brightest arc of Sun sliver)

Point S_1 is at the center of the arc $\widehat{AS_1B}$ and is positioned at the Sun sliver width. Therefore, it is collinear with the Moon's center M and the Sun's center C .

Let's denote the projection of point O toward disks.

O' - projection of point O onto the plane of the Sun and Moon disks

Since points O, C', M' are collinear, the points O', C, M along with point S_1 also must be collinear.

Corollary 1 *Projections of the Sun's center, Moon's center, Sun sliver width, and observation surface's center onto the plain of the observation surface are collinear.*

Point S_1 is the brightest location on the Sun sliver and the closest point of the Sun base to the observation surface point O . It projects light with maximum efficiency due to beaming angle.

As a result, point S_1 along with the surrounding domain of the Sun sliver base and the width, has the strongest illumination effect on the observation surface. The farther a Sun sliver point is from this domain, the weaker its illumination on the observation surface becomes.

The closest point on the Chromosphere sliver base to the observation surface also projects light the most effectively. This point is collinear with the Sun and Moon centers. A similar principle applies to the brightest point on the Corona sliver base, which also aligns along the same collinear path.

S_2 - Chromosphere sliver base point closest and brightest to points O' and O
 S_3 - Corona sliver base point closest and brightest to points O' and O

The domains of the Chromosphere and Corona sliver bases respectively surrounding points S_2 and S_3 , exert the strongest illumination effect on the observation surface.

The observation surface's diameter is several orders of magnitude smaller than the umbra circumference, measuring thousands of times less in length. If a circular arc was that small compared to the full circle's circumference, it would appear as a straight line. Similarly, the three sliver domains can be interpreted as shafts of light.

Projections of these three shafts of light toward umbra are three shafts around point O .

S'_1, S'_2, S'_3 - projections respectively of points S_1, S_2, S_3 toward umbra

1. The Sun shaft of light around point S_1 projects onto the shaft around point S'_1 .
2. The Chromosphere shaft of light around point S_2 projects onto the shaft around point S'_2 .
3. The Corona shaft of light around point S_3 projects onto the shaft around point S'_3 .

These shafts dominate illumination on the observation surface. To emphasize their influence in both FIGURES 3, 4, these shafts are thickened. In addition, as totality approaches and the Moon gets close to the Sun edge, all three slivers get shorter as the impact of all three shafts gets pronounced. In total solar eclipses the Moon disk is greater than the Sun disk. When the size difference is emphasized, all three slivers are somewhat smaller making the shafts influence even greater.

While it is known that Earth revolves around the Sun, the Sun appears to move across the sky, from the Earth-based perspective. Therefore, the Sun's center motion is depicted with a vector in FIGURE 3.

Notice that between the Sun shaft of light and Chromosphere shaft of light there is the Dark Band shaft of light. And so, there is the Transition Region shaft between the Chromosphere and Corona shafts of light.

The Dark Band and Transition Region shafts of light are not graphed in the illustrations (FIGURES 3, 4) due to their small illumination impact. In a more detailed analysis, their contributions will be incorporated into the overall illumination model, providing a more comprehensive understanding.

It is important to note that all shafts from point O are positioned tangentially at the appropriate points along the arcs of the circles and ellipse in FIGURES 3, 4. This means that

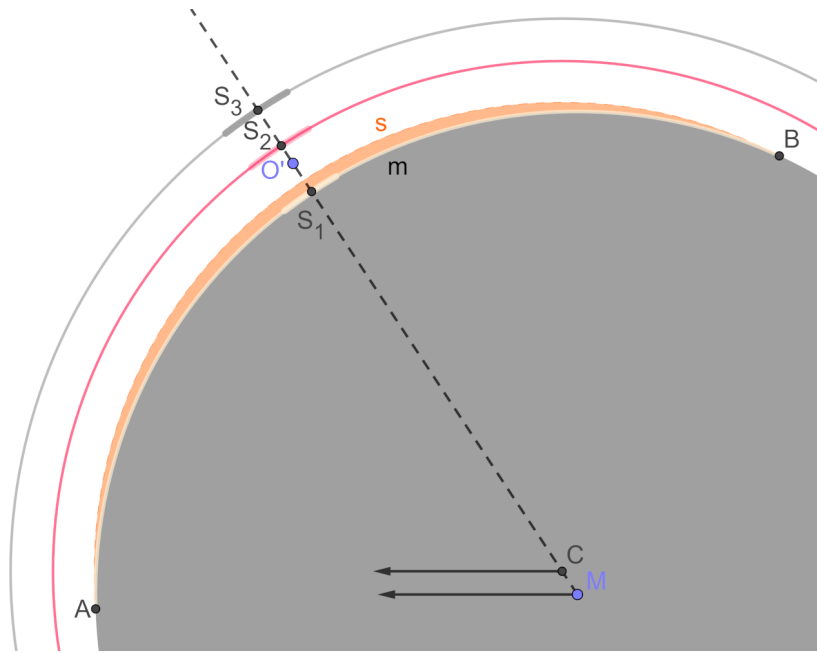


Figure 3: Domains and Shafts

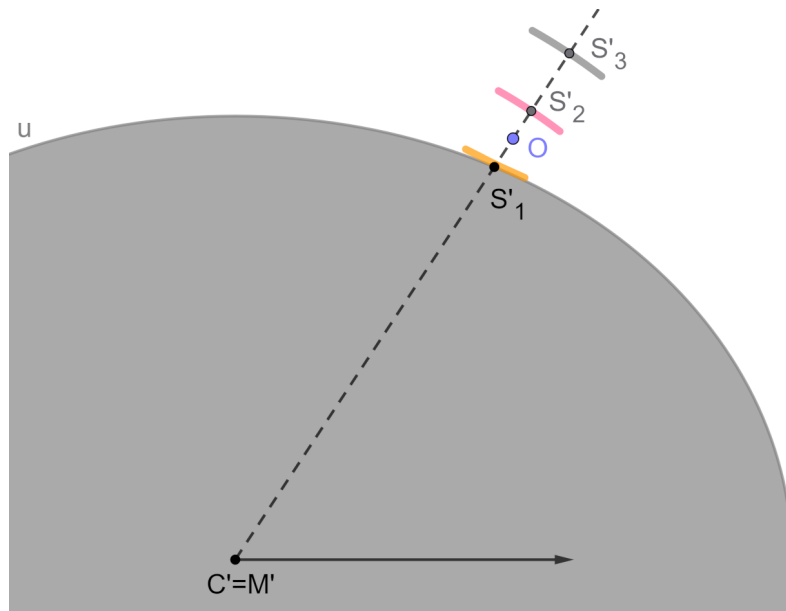


Figure 4: Projection on Observation Surface Plane

all three shafts of light on the observation surface are tangential to the Sun and Moon disks, as well as to the umbra.

Let's denote the Sun sliver's width.

w - Sun sliver's width

S - Sun surface point at w

In FIGURE 3 of domains and shafts it means that

$$S_1S = w$$

Segment SS_2 is the distance from the Sun surface to the Chromosphere base that we already estimated:

$$SS_2 = \delta_3$$

Segment S_2S_3 is the distance from the Chromosphere base to the Corona base that we also already approximated:

$$S_2S_3 = d_1$$

Case 2 *This document explores the essential characteristics of shadow bands, assuming the observation surface lies near the umbra centerline.*

When the observation surface is positioned along the centerline of the umbra, the Sun sliver's width along with other collinear points are also onto the direction of centerline (FIGURE 5). As a result, the shafts of light from the Sun, Chromosphere, and Corona are all perpendicular to the centerline.

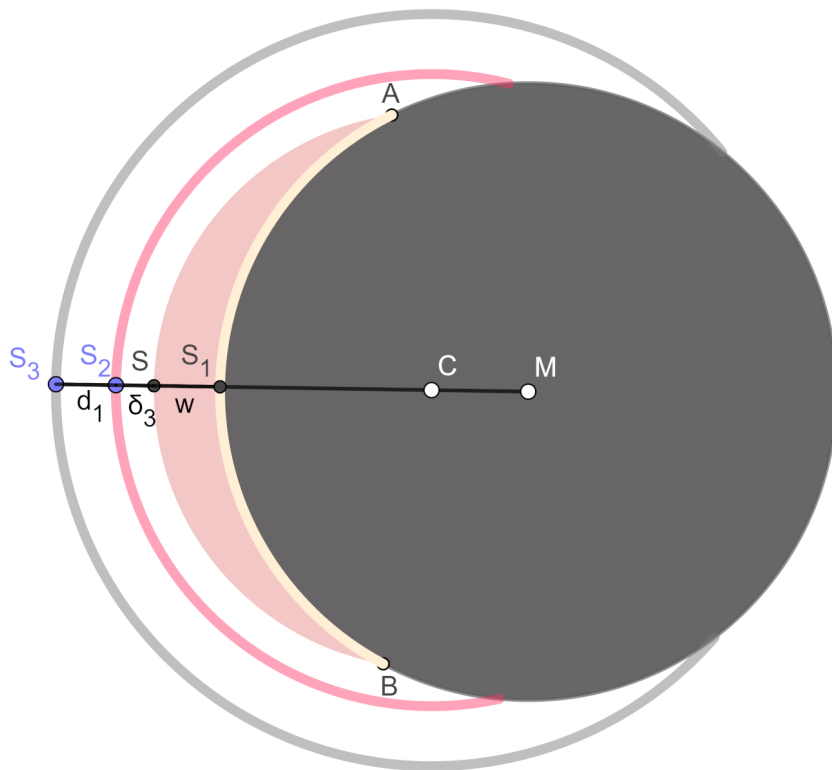


Figure 5: Triple-sliver when Observation Surface at Centerline

As the Sun sliver's width (w) shrinks, point S_1 moves along the Moon's edge, and on the verge of totality reaches the Sun surface point S .

Shadow bands occur at various moments leading up to totality, typically appearing earlier and later than one minute before, but rarely beyond a few minutes before totality. This makes one minute before totality a reliable reference point. We'll start by determining the Sun sliver's size exactly one minute before totality. Once established, we'll then calculate how its width varies at different moments.

1 minute before totality

$$w = ?$$

Since the Sun's diameter is known, determining the Sun sliver's width as a fraction of the diameter will reveal how many times the sliver's width is smaller in comparison. This ratio provides a useful reference for scaling its size relative to the full Sun.

To simplify calculations while maintaining accuracy, we'll use the fact that the Sun's diameter is relatively small compared to its distance to Earth. This allows for effective approximations without significant loss of precision.

z - distance from Sun to Earth

$$\begin{aligned} z &= 1.5 \times 10^8 \text{ km} \\ &= 150\,000 \text{ Mm} \\ \frac{2R}{z} &= \frac{1\,400 \text{ Mm}}{150\,000 \text{ Mm}} < 1\% \end{aligned}$$

Given the relatively constant speed of the Moon's and Earth's revolutions and rotations, we assume that the cumulative angular speed of the Moon's disk remains constant relative to the Sun-Earth axis.

As the observation surface is on the centerline, the Moon's center passes directly over the Sun's center from Earth perspective. This implies that the angular sizes are proportional to the corresponding eclipse durations. Consequently, we can determine the ratio of angular sizes using the ratio of their respective durations.

Eclipsing of the Sun sliver by the Moon takes one minute, as we have chosen. The eclipsing of the entire Sun begins at C1 (start of eclipse) and ends at C2 (total eclipse)—a phase known as the *(first) partial phase*.

Based on statistical observations, the partial phase typically lasts between 70 and 80 minutes. To establish a reasonable estimate, we select 75 minutes, positioned near the midpoint of this range.

$$\begin{aligned} \frac{w}{2R} &= \frac{1}{75} \\ w &= \frac{2R}{75} \end{aligned}$$

We found that one minute before totality the Sun sliver's width is one 75th of the Sun's diameter. Let's find the percentage.

$$\frac{1}{75} = \frac{100\%}{75} = 1.33\%$$

The Sun sliver's width fraction of the Sun's diameter, combined with the fraction of the Sun's diameter covered by the Moon, together account for the entire Sun's diameter.

The fraction of the Sun's diameter covered by the Moon is known as *eclipse magnitude*—a key measure in describing the extent of the eclipse.

μ - eclipse magnitude (Sun diameter fraction covered by the Moon)

$1 - \mu$ - Sun sliver's width fraction (Sun diameter fraction not covered by the Moon)

$$\frac{w}{2R} = 1 - \mu$$

If given eclipse magnitude, then we can calculate the Sun sliver's width with the formula

$$w = (1 - \mu) \cdot 2R \quad (1)$$

Let's find the eclipse magnitude and the Sun sliver's width fraction at various moments below totality.

1 minute before totality

$$\begin{aligned} \mu &= 100\% - 1.33\% \\ &\approx 98.67\% \end{aligned}$$

At three minutes before totality—when shadow bands may start to appear—the Sun sliver's width is 4% of the Sun's diameter. At this moment, the Moon has covered the entire Sun, except for the darkened limb. This suggests a correlation between limb darkening and shadow bands formation.

Having specific time moments before totality can serve as a framework for our analysis. These moments, listed in the first column of TABLE 1 below, represent time measured in seconds or minutes before C2 event.

t - time before totality

We calculate the eclipse magnitude for each moment from the first column of the table and list it in the second column as a percentage.

To determine the Sun sliver's width values, we apply the formula from EQUATION 1 above that substitutes the eclipse magnitudes from the second column and the known Sun's diameter. The Sun sliver's width values are listed in the third column of the table, provided in megameters (Mm) and rounded to two decimal places.

The distance between two bright point sources of light S_1 and S_2 from shafts is

$$S_1S_2 = S_1S + SS_2$$

d_3 - distance from Sun shaft to Chromosphere shaft

$$S_1S_2 = d_3$$

$$d_3 = w + \delta_3$$

The distance d_3 is dynamic and it calculates by increasing the width w from the third column with the known distance δ_3 .

$$\delta_3 = 0.9 \text{ Mm}$$

We list its values in the fourth column of the table. On the verge of totality, the distance d_3 shrinks to the distance between Sun shaft and Chromosphere shaft, that is δ_3 .

$$w = 0 \implies d_3 = \delta_3$$

The distance between the Corona shaft and Sun shaft is determined by summing the distances from Corona shaft to Chromosphere shaft, and from Chromosphere shaft to Sun shaft:

$$S_1S_3 = S_1S_2 + S_2S_3$$

d_2 - distance from Corona shaft to Sun shaft

$$S_1 S_3 = d_2$$

$$d_2 = d_3 + d_1$$

The distance d_2 is dynamic. We calculate the distances by increasing the distance d_3 from the fourth column with the constant and known distance d_1 .

$$d_1 = 1.6 \text{ Mm}$$

We list the values in the fifth and final column of the table. Let's outline our celestial triple-silver distances.

d_3 - distance from Sun shaft to Chromosphere shaft

d_1 - distance from Chromosphere shaft to Corona shaft

d_2 - distance from Corona shaft to Sun shaft

Table 1: Triple-silver Distances over Time

| t | μ | w | d_3 | d_2 |
|--------|-------|-------|-------|-------|
| 0 s | 100 | 0 | 0.90 | 2.50 |
| 5 s | 99.89 | 1.54 | 2.44 | 4.04 |
| 10 s | 99.78 | 3.08 | 3.98 | 5.58 |
| 20 s | 99.56 | 6.17 | 7.07 | 8.67 |
| 30 s | 99.33 | 9.25 | 10.15 | 11.75 |
| 40 s | 99.11 | 12.33 | 13.23 | 14.83 |
| 50 s | 98.89 | 15.42 | 16.32 | 17.92 |
| 1 min | 98.67 | 18.50 | 19.40 | 21.00 |
| 2 min | 97.33 | 37.00 | 37.90 | 39.50 |
| 3 min | 96.00 | 55.50 | 56.40 | 58.00 |
| 4 min | 94.67 | 74.00 | 74.90 | 76.50 |
| 5 min | 93.33 | 92.50 | 93.40 | 95.00 |
| s, min | % | Mm | Mm | Mm |

We may conclude that, to a rough approximation, the Chromosphere and Corona shafts act geometrically as a single shaft of light up to a dozen seconds before totality.

At a specific moment during a total solar eclipse, three shafts of light—from the Sun, Chromosphere, and Corona—are geometrically defined by the observer's location (see FIGURES 3, 4 on P. 13).

The Sun shaft of light, directed toward the observation surface, can be interpreted as light passing through one slit in a celestial-scale double-slit "experiment." Similarly, the Chromosphere shaft of light acts as the second slit. The observation surface serves as the screen, or a small portion of it, where interference pattern may emerge in the form of fringes.

We thus recognize elements of the double-slit experiment on a cosmic scale, referring to this configuration as the *Sun & Chromosphere-silver "experiment"* or as the *celestial double-silver "experiment."*

However, this is not a static "experiment." As totality approaches, the Sun sliver—the brightest and most dominant—changes in width and intensity, rendering one of the "slits" dynamic. This transforms the analogy into a variable-slit interference model, where fringe behavior evolves in real time.

The Corona sliver, being the dimmest and spatially comparable to the Chromosphere sliver, introduces a third shaft of light. For simplicity, it is excluded from the analysis.

4 Predictions

A star consists of an immense number of emitters, each radiating light at random intervals. Consequently, lights from two separate points on the star’s surface are completely uncorrelated—both spatially and temporally incoherent.

This stands in contrast to setups like the double-slit experiment, where coherence is preserved by design. In the stellar case, no fixed phase relationship exists between photons emitted from neighboring regions.

However, as starlight propagates over astronomical distances, its spatial coherence evolves. Despite a star’s large diameter, its vast remoteness causes it to act, from our viewpoint, as a quasi-point source. Just as stars appear as tiny specks in the night sky, their light behaves coherently upon arrival at Earth.

During a solar eclipse, the coherence dynamics shift. As the Moon obscures the Sun, only a narrow sliver of the solar disk remains visible—just before and after totality. At these moments, the ratio of the sliver’s angular width to its distance from Earth becomes dramatically small, which can induce a transition toward coherence.

Now, we examine the spatial and temporal coherence in our celestial double-sliver “experiment.” In addition, we’ll estimate the fringe width and spacing based upon the spatial coherence length.

Normal sunlight is broadband, which results in low temporal coherence. However, during an eclipse, this may change due to specific optical effects introduced by the event. To analyze this shift, we will compare the coherence of normal sunlight with that of the Sun & Chromosphere-sliver.

As totality approaches, the Sun sliver’s width—and consequently its angular width—diminishes significantly. Three minutes before totality, our calculations show that the Sun sliver’s width is about 4% of the Sun’s diameter; one minute before totality, it narrows farther to 1.33%. On the verge of totality, the sliver shrinks to none. This dramatic reduction greatly enhances spatial coherence, as the Sun’s angular size is large in comparison to the progressively smaller sliver’s widths.

Thus, after a certain moment leading up to totality, the Sun shaft of light should exhibit high spatial coherence. And even a few minutes before totality, it should maintain at least partial coherence, given the tiny remaining sliver.

Additionally, the greatest illumination effect arises from the Sun sliver base and its width, which constitutes only a small distance portion of the crescent width.

The bright Chromosphere (excluding the Dark Band) can extend up to 2 000 km, though it is typically thinner. Now, we estimate its ratio relative to the Sun’s diameter:

$$\frac{2\,000\text{ km}}{2R} = \frac{2\text{ Mm}}{2 \cdot 700\text{ Mm}} < 0.2\%$$

Our calculations show that one minute before totality, the Chromosphere sliver’s width is less than 0.2% of the Sun’s diameter. However, due to the dynamic nature of the Chromosphere, this width could be several times shorter.

Compared to normal sunlight, the spatial coherence of the Chromosphere light is significantly better. Additionally, the greatest illumination effect arises from the Chromosphere sliver base, which constitutes only a portion of the entire Chromosphere sliver.

Since the Dark Band is generally narrower than the Chromosphere base, the combined spatial coherence of the Sun and Chromosphere slivers—and especially shafts of light—far exceed that of normal sunlight.

One minute before totality, the Moon obscures the Sun, except for the Sun limb zone, which remains visible as the Moon enters it.

As previously noted, when discussing limb darkening, the Sun sliver exhibits both broadband and discrete spectral characteristics. The greater limb darkening means enhancing the discrete spectrum of the Sun atmosphere over broadband spectrum of the Sun surface.

- The broadband spectrum reduces coherence.
- The discrete spectrum enhances coherence.

Therefore, the limb darkening effect significantly enhances temporal coherence.

On the verge of totality, due to maximal limb darkening, the Sun sliver’s temporal coherence quality reaches its maximum.

The Chromosphere spectrum is quasi-monochromatic, making it far more temporally coherent than the broadband spectrum of normal sunlight.

As the Sun sliver narrows, the influence of discrete Chromosphere wavelengths becomes more pronounced on the Sun sliver, leading to the Chromosphere spectral characteristics appearing on both slivers. Since two light sources sharing the same discrete wavelengths enhance overall temporal coherence, the combined effect of the Sun & Chromosphere-sliver—and particularly shafts of light—significantly improve temporal coherence as totality approaches.

On the verge of totality, the combined temporal coherence reaches its maximum.

All the preceding observations support the conclusion that light coherence is significantly enhanced when the Sun sliver is within the Sun limb region, occurring a few minutes before totality. As totality approaches, the coherence of the Sun & Chromosphere-slivers increase steadily, reaching its maximum on the verge of totality.

Thus, the combined potential of the Sun & Chromosphere-slivers, and especially shafts of light, to generate interference fringes is substantially greater than that of the entire Sun.

Although the width and optical quality of the celestial "slits" are not examined in detail here, it is worth noting that in several key respects these naturally formed slits, despite their heterogeneous origin, outperform the simple apertures employed in Young’s demonstration.

Given that the Sun & Chromosphere-sliver is expected to generate fringes, a key question arises regarding fringe width and spacing. As established, in a double-slit experiment, when the slit separation matches the spatial coherence length, the fringe width and spacing near the central axis closely align with the spatial coherence length itself.

The experimental results presented by Mashaal et al. (2012) in their proceedings *Spatial coherence of sunlight: first direct measurement* confirm previously established theoretical predictions regarding the spatial coherence of sunlight [19]. The theoretical prediction is that for an average wavelength of 510 nm the spatial coherence length of sunlight is approximately 50 μm at the Earth’s surface under clear skies. However, if the Earth’s atmosphere causes cloudy and foggy weather, the spatial coherence length may decrease even a dozen times.

If the Moon or another object were to obscure the Sun, leaving only two diametrically opposite points exposed, these two point-sources of light would generate an interference pattern. When filtered to match the average solar wavelength, the resulting fringes would exhibit a width and spacing of 50 μm just like in theoretical and experimental predictions.

In our double-sliver “experiment,” the distance between the Sun and Chromosphere sliver bases five seconds before totality is estimated at

$$d_3 = 2.4 \text{ Mm}$$

Compared to the Sun’s diameter, the distance between slivers is smaller by a factor evaluated as follows:

$$\frac{2R}{d_3} = \frac{2 \cdot 700 \text{ Mm}}{2.4 \text{ Mm}} \approx 600$$

Therefore, the fringe width and spacing in our double-sliver “experiment” are 600 times greater than 50 μm due to the inverse proportionality, but for the average sunlight.

Therefore

$$600 \cdot 50 \mu\text{m} = 3 \text{ cm}$$

To refine this further, we will also account for the effect of wavelength on our calculations. So, let's determine the wavelength relevant to our celestial double-sliver "experiment."

The strongest spectral line of the Corona is very close to the strongest line of the Chromosphere, reinforcing coherence effects. One sliver originates from the Chromosphere, while the other becomes like the Chromosphere on the verge of totality. As a result, the Chromosphere spectrum plays a major role in shaping fringe formation.

Meanwhile, Dark Band remains significantly dim compared to these two approximately equal dominant spectral lines.

λ - wavelength of celestial double-sliver "experiment"

$$\begin{aligned} \lambda &\approx 656.3 \text{ nm} \\ &\approx 637.4 \text{ nm} \\ &\approx 650 \text{ nm} \end{aligned}$$

Due to proportionality, the fringe width and spacing can be calculated as follows:

$$\begin{aligned} \frac{650 \text{ nm}}{510 \text{ nm}} \cdot 3 \text{ cm} &= \frac{65}{51} \cdot 3 \text{ cm} \\ &\approx \frac{68}{17} \text{ cm} \\ &\approx 4 \text{ cm} \end{aligned}$$

The formula for the fringe width and spacing yields almost the same result.

z - distance from slits to screen

d - distance between slits

$$\begin{aligned} \frac{\lambda z}{d} &= \frac{650 \text{ nm} \cdot 150\,000 \text{ Mm}}{2.4 \text{ Mm}} \\ &= \frac{6.5 \cdot 10^2 \cdot 10^{-9} \text{ m} \cdot 1.5 \cdot 10^5}{2.4} \\ &= \frac{6.5 \cdot 1.5}{2.4} \cdot 10^{-2} \text{ m} \\ &\approx 4 \text{ cm} \end{aligned}$$

Conclusion 3 *The fringe width and spacing above the Earth's atmosphere or on the ground under clear skies are approximately 4 cm.*

This estimated fringe width and spacing closely align with the shadow band width and spacing.

From the geometric model we infer that the interference fringes are concentric with the umbra and therefore appear locally as lines tangential to its boundary. They are generated way above the Earth atmosphere. They move along the umbra at speeds far too great for photographic cameras to capture effectively. The other observational constraints can be demonstrated without substantial complication.

5 Conclusions and Discussion

When we restate all dark fringe distinct properties emerging from the celestial triple-sliver light interference pattern, we recognize that they match those of shadow bands: their appearance, size, speed, direction, duration, and more. We supposed that dark fringes and shadow bands are one and the same phenomenon, and now we confirm that it is true.

Therefore, any conclusions we've drawn about dark fringes apply directly to shadow bands.

From this point forward, we will avoid referring to them as “dark fringes” or “hypothetical shadow bands.” Instead, we will use the unified scientific term: shadow bands.

Let us recall that shadow bands are not exclusive to total solar eclipses. While our focus has been on the Sun as the source, other stars—provided they exhibit sufficient light coherence—could also produce them.

For this to occur, such stars must possess bright ring-like structures and intervening dark layers within their atmospheres. These features would mirror the Sun's architecture: the luminous bases of the Chromosphere and Corona, separated by the obscuring strata of the Dark Band and the Transition Region.

Definition 4 *Shadow bands* are dark fringes that may appear on an observation surface when a star's disk is nearly obscured. They arise from the star's dark limb zone and at least one bright sliver-like atmospheric layer, flanked by adjacent dark regions. This configuration mostly induces light interference from the brightest regions around sliver centers that act as shafts of light, much like slits beam in a classical multiple-slit experiment.

Definition 5 *Solar shadow bands* mostly emerge due to the light interference from the shafts of the Sun, Chromosphere, and Corona-sliver bases—a celestial analogue of a triple-slit experiment—activated when the Sun nearly eclipses. These luminous regions are embedded within the darker surroundings of the Dark Band and the Transition Region.

Corollary 6 *Because the Corona base is relatively dim and closely aligned with the Chromosphere base, the resulting interference may be approximated as a Sun & Chromosphere-sliver pattern.*

When conceptually dilated, this celestial double-sliver "experiment" becomes comparable to Young's double-slit experiment as dynamic nature variant, revealing the deep symmetry between celestial and laboratory-scale interference.

We can simplify the causation of the solar shadow bands in a sentence easy to remember:

Summary 7 *Dark bands of a solar eclipse are caused by the Dark Band.*

The appearance of shadow bands is governed by a complex interplay of factors, including:

- the width and dynamics of solar layers near the limb,
- the degree of partial light coherence in the incoming light,
- the structural features of the umbra, and
- the conditions of Earth's atmosphere, such as turbulence, refractive gradients, and surface reflectivity.

As a result, shadow bands exhibit highly dynamic and inherently unpredictable behavior, varying not only from eclipse to eclipse but even from moment to moment within a single event.

Additional material relevant to these conclusions—including extended derivations and supplementary observational data—is available in the author's book *The Optics of Shadow Bands: Causation and Effect* (2025) [20].

References

- [1] Abbe, C. (1900). Eclipse shadow bands and correlated atmospheric phenomena, *Monthly Weather Review* **28**, 5, p. 210.
- [2] Alissandrakis, C. E. and Macris, C. J. (1971). A study of the fine structure of the solar chromosphere at the limb, *Solar Physics* **20**, 1, pp. 52–53, doi:10.1007/bf00146093, URL <https://ui.adsabs.harvard.edu/abs/1971SoPh...20...47A/abstract>.
- [3] British Astronomical Association (1906). *The total solar eclipse 1905: Reports of observations made by members of the British Astronomical Association* (British Astronomical Association, London), URL <https://archive.org/details/totalsolareclips00britrich>, observational report of the August 30, 1905 total solar eclipse. Public domain.
- [4] Codona, J. L. (1986). The scintillation theory of eclipse shadow bands, *Astronomy and Astrophysics* **164**, 2, pp. 415–427, URL <https://articles.adsabs.harvard.edu/full/1986A&A...164..415C>, please note that the article is copyrighted and may not be freely reproduced.
- [5] Codona, J. L. (1991). The enigma of shadow bands, *Sky and Telescope* **81**, 5, pp. 482–487.
- [6] Feldman, R. L. (1938a). Shadow bands – Part I, *Popular Astronomy* **46**, pp. 187–200, URL <https://adsabs.harvard.edu/full/1938PA....46..187F>, this article is believed to be in the public domain.
- [7] Feldman, R. L. (1938b). Shadow bands – Part II, *Popular Astronomy* **46**, pp. 263–273, URL <https://articles.adsabs.harvard.edu/full/1940PA....48...2F>, this article is believed to be in the public domain.
- [8] Feldman, R. L. (1940). Shadow bands – Part III, *Popular Astronomy* **48**, p. 182, URL <https://articles.adsabs.harvard.edu/full/1940PA....48..182F>, this article is believed to be in the public domain.
- [9] Feldman, R. L. (1974). On shadow bands accompanying total solar eclipses, *American Journal of Physics* **42**, 11, pp. 1024–1026, doi:10.1119/1.1987919.
- [10] Gaviola, E. (1948). On shadow bands at total eclipses of the sun, *Popular Astronomy* **56**, pp. 353–359, URL <https://ui.adsabs.harvard.edu/scan/manifest/1948PA....56..353G>, this article is believed to be in the public domain.
- [11] Gladysz, S., Redfern, M. and Jones, B. W. (2005). Shadow bands observed during the total solar eclipse of 4 December 2002, by high-resolution imaging, *Journal of Atmospheric and Solar-Terrestrial Physics* **67**, 10, pp. 899–906, doi:10.1016/j.jastp.2005.02.012.
- [12] Henry, A. J. (1906). Observations of “shadow bands” without an eclipse, *Monthly Weather Review* **34**, 5, p. 227.
- [13] Hults, M. E., Burgess, R. D., Mitchell, D. A. and Warn, D. W. (1971). Visual, photographic and photoelectric detection of shadow bands at the March 7, 1970, solar eclipse, *Nature* **231**, 5300, pp. 255–258, doi:10.1038/231255a0.
- [14] Jones, B. W. (1996). Shadow bands during the total solar eclipse of 3 November 1994, *Journal of Atmospheric and Terrestrial Physics* **58**, 12, pp. 1309–1316, doi:10.1016/0021-9169(95)00162-x.

- [15] Jones, B. W. and Jones, C. (1994). Shadow bands during the total solar eclipse of 11 July 1991, *Journal of Atmospheric and Terrestrial Physics* **56**, 12, pp. 1535–1543, doi:10.1016/0021-9169(94)90082-5.
- [16] Klement, G. T. (1974). Observations of short term light variations during the June 30, 1973 solar eclipse, *Astronomy and Astrophysics* **37**, 2, pp. 431–433, URL <https://articles.adsabs.harvard.edu/full/1974A&A....37..431K>.
- [17] Madhani, J. P., Chu, G. E., Gomez, C. V., Bartel, S., Clark, R. J., Coban, L. W., Hartman, M., Potosky, E. M., Rao, S. M. and Turnshek, D. A. (2020). Observation of eclipse shadow bands using high altitude balloon and ground-based photodiode arrays, *Journal of Atmospheric and Solar-Terrestrial Physics* **211**, 105420, doi:10.1016/j.jastp.2020.105420, preprint available on arXiv site (not in the public domain).
- [18] Marschall, L. A. (1984). Shadow bands – Solar eclipse phantoms, *Sky and Telescope* **67**, p. 116.
- [19] Mashaal, H., Goldstein, A., Feuermann, D. and Gordon, J. M. (2012). Spatial coherence of sunlight: first direct measurement, in R. Winston and J. M. Gordon (eds.), *Nonimaging Optics: Efficient Design for Illumination and Solar Concentration IX*, Vol. 8485 (SPIE), p. 84850A, doi:10.1117/12.928449.
- [20] MathallicA (2025). *The optics of shadow bands: Causation and effect*, 1st edn. (MathallicA), ISBN 978-86-908194-0-9, URL <https://www.amazon.com/dp/8690819401/>, paperback edition.
- [21] O’Meara, S. J. (2009). Secret sky – Searching for shadow bands, *Astronomy* **37**, 4, pp. 18–19, URL <https://www.astronomy.com/observing/stephen-james-omearas-secret-sky-searching-for-shadow-bands/>.
- [22] Rotch, A. L. (1908). The eclipse shadow-bands, *Annals of the Astronomical Observatory of Harvard College* **58**, pp. 217–222, URL <https://adsabs.harvard.edu/full/1908AnHar..58..217R>.
- [23] Schawlow, A. L. (1968). Laser light, *Scientific American* **219**, 3, pp. 120–136.
- [24] Seykora, E. J. (1979). Observations of eclipse shadow bands and related phenomena, *Applied Optics* **18**, 21, pp. 3538, 3539, doi:10.1364/ao.18.003538.
- [25] Watts, H. M. (1925). Shadow bands during the period of greatest obscuration, January 24, 1925, *Popular Astronomy* **33**, p. 236, URL <https://articles.adsabs.harvard.edu/pdf/1925PA....33..236W>, public domain.